

Article

## Orientation and Temperature Dependence of Piezoelectric Properties for Sillenite-Type $\text{Bi}_{12}\text{TiO}_{20}$ and $\text{Bi}_{12}\text{SiO}_{20}$ Single Crystals

Chuanying Shen <sup>1,2</sup>, Huaijin Zhang <sup>1,\*</sup>, Yuanyuan Zhang <sup>1</sup>, Honghao Xu <sup>1</sup>, Haohai Yu <sup>1</sup>, Jiyang Wang <sup>1</sup> and Shujun Zhang <sup>2,\*</sup>

<sup>1</sup> State Key Laboratory of Crystal Materials, Institute of Crystal Materials, Shandong University, Jinan 250100, Shandong, China; E-Mails: chuanyingshen@gmail.com (C.S.); zhangyuanyuan@sdas.org (Y.Z.); honghaoxu11@gmail.com (H.X.); haohaiyu@sdu.edu.cn (H.Y.); jyywang@sdu.edu.cn (J.W.)

<sup>2</sup> Materials Research Institute, Pennsylvania State University, University Park, PA 16802, USA

\* Authors to whom correspondence should be addressed; E-Mails: huaijinzhang@sdu.edu.cn (H.Z.); soz1@psu.edu (S.Z.); Tel.: +86-531-883-64686 (H.Z.); +1-814-863-2639 (S.Z.); Fax: +86-531-885-74135 (H.Z.).

Received: 30 April 2014; in revised form: 22 May 2014 / Accepted: 28 May 2014 /

Published: 20 June 2014

---

**Abstract:** The full matrix of electro-elastic constants of sillenite-type crystals  $\text{Bi}_{12}\text{TiO}_{20}$  (BTO) and  $\text{Bi}_{12}\text{SiO}_{20}$  (BSO) were determined by the resonance method, with  $d_{14}$  and  $k_{14}$  being on the order of 40–48 pC/N and 31%–36%, respectively. In addition, double-rotated orientation dependence of  $d_{33}$  was investigated, with the maximum values of 25–28 pC/N being achieved in  $XZ\text{t}l45^\circ/54^\circ$ -cut samples. The electrical resistivity of BSO was found to be two orders higher than that of BTO, being on the order of  $7 \times 10^5 \Omega \text{ cm}$  at 500 °C. The temperature dependence of dielectric and piezoelectric properties were investigated. BSO exhibited a high thermal stability in the temperature range of 25–500 °C, while BTO showed a variation of ~3% in the range of 25–350 °C. The high values of  $d_{14}$  and  $k_{14}$ , together with the good thermal stability, make BTO and BSO crystals potential candidates for electromechanical applications in medium temperature range.

**Keywords:** sillenite-type crystals; piezoelectric; orientation dependence; thermal stability

---

## 1. Introduction

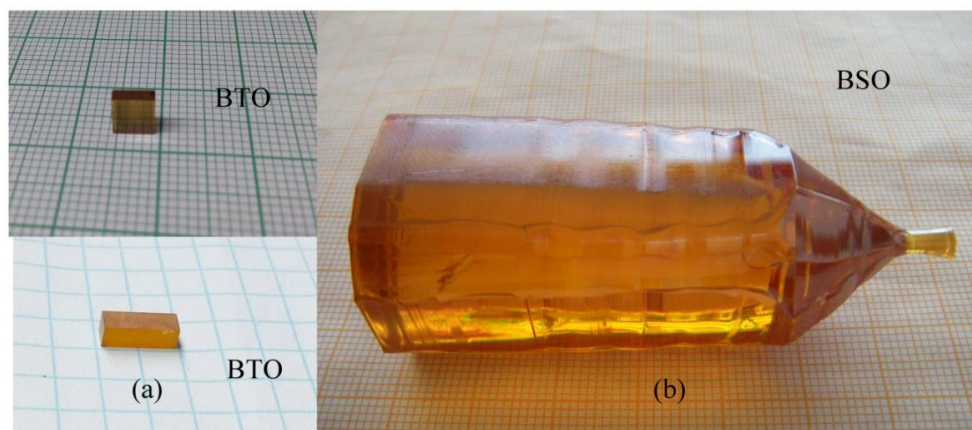
Sillenite-type  $\text{Bi}_{12}\text{MO}_{20}$  (where  $M = \text{Ti, Si and Ge}$ , known as BTO, BSO and BGO) crystals have non-centrosymmetric, body-centered cubic structure belonging to the I23 space group [1,2]. The structure of sillenite-type crystals was first determined by Sillen [3] and later refined by Efendiev and Wiehl [4,5]. Due to the space group, these crystals present a number of remarkable properties, such as piezoelectric, electro-optic, elastic-optic and photoconductive properties, which have potential applications in spatial light modulators, acoustic delay lines, for hologram recording and phase conjugation [6–12]. Of particular importance is that these crystals are piezoelectric semiconductors with large piezoelectric constant ( $d_{14} \sim 40$  pC/N), large electromechanical coupling factor ( $>30\%$ ), large band gap energy (3.15–3.25 eV) and fast response time [6,13], in addition, there is no ferroelectric and pyroelectric properties, related to the 23 point group.

Extensive research has been carried out on the optical and room temperature piezoelectric properties of sillenite-type crystals [8,13–15]. However, studies on the piezoelectric properties as a function of orientation and temperature are limited. In this study, the full matrix of electro-elastic constants of  $\text{Bi}_{12}\text{TiO}_{20}$  (BTO) and  $\text{Nd}_{0.06}\text{Bi}_{11.94}\text{SiO}_{20}$  (abbreviated as Nd: BSO or BSO) crystals were determined using resonance method based on IEEE Standards on Piezoelectricity. The piezoelectric coefficient  $d_{14}$  and coupling factor  $k_{14}$  of BTO were calculated by two methods: length extension and face shear vibrations, respectively. The double-rotated orientation dependence of longitudinal piezoelectric response was analyzed. Furthermore, the temperature dependence of electrical resistivity, dielectric, elastic, electromechanical coupling and piezoelectric constants were investigated in the range of 25–500 °C.

## 2. Results and Discussions

Figure 1a shows part of the samples cut from BTO single crystals used for electrical study. The as-grown BSO crystal [16] with dimensions of  $\phi 30 \times 45 \text{ mm}^3$  was given in Figure 1b, which was pulled along [110] crystallographic direction.

**Figure 1.** (a) The  $\text{Bi}_{12}\text{TiO}_{20}$  (BTO) samples; (b) The as-grown  $\text{Bi}_{12}\text{SiO}_{20}$  (BSO) single crystal pulled along [110] direction.



### 2.1. Room Temperature Material Constants

The dielectric, elastic and piezoelectric constants of the BTO and BSO single crystals were measured by resonance method, as listed in Table 1 (different samples were measured and the errors were found to be low, being less than 5%), and compared to the reported values measured by the ultrasonic method [8,13]. It is clear that the results are in good agreement with those obtained by the ultrasonic method, with piezoelectric coefficient  $d_{14}$  of BSO larger than the reported values, which may be induced by the Nd dopant. In addition, the  $d_{14}$  and  $k_{14}$  of BTO crystals were measured by face shear vibration mode directly, the values were found to be on the order of 40.7 pC/N and 31.0%, respectively, being similar to those values measured by length extension mode (42.8 pC/N and 32.8%). BTO and BSO possess similar physical properties, due to the fact that the body-centered cubic sillenite-type structure can accommodate a variety of different M ions, and the oxygen tetrahedron is able to expand or contract without a major effect on the remaining atomic arrangement [2].

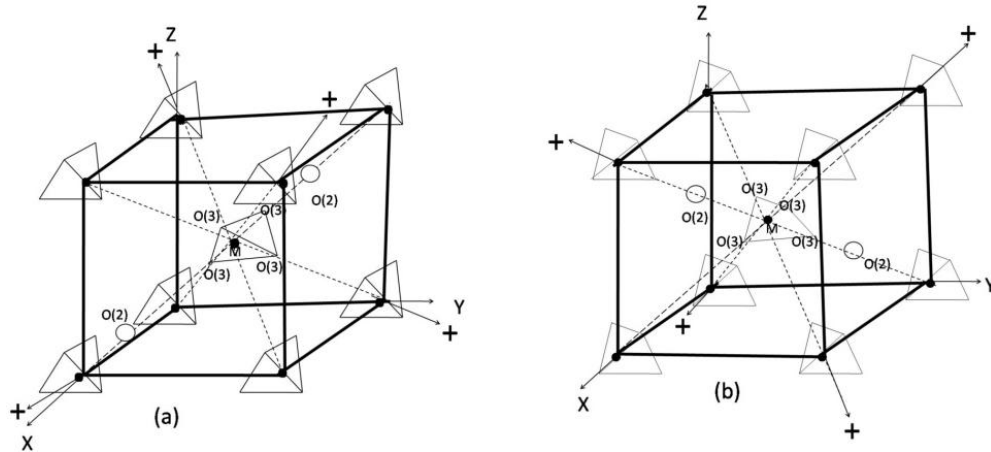
**Table 1.** Room temperature electro-elastic constants for BTO and BSO crystals.

Electro-Elastic Constants	Symbols	BTO	BTO [8]	BSO	BSO [13]
Relative Dielectric Permittivities	$\epsilon_{11}$	47.9	47.0	48.2	47.0
Dielectric Loss	$\tan\delta$	0.01%	–	0.09%	–
Elastic Compliance Constants $s^E$ ( $\text{pm}^2/\text{N}$ )	$s_{11}$	9.8	8.7 *	10.3	8.5
	$s_{12}$	–1.8	–1.6 *	–2.7	1.5
	$s_{44}$	40.3	40.7 *	40.4	40.0
	$c_{11}$	11.2	12.5	11.9	12.8
Elastic Stiffness Constants $c^E$ ( $10^{10}$ N/m <sup>2</sup> )	$c_{12}$	2.6	2.8	4.3	2.8
	$c_{44}$	2.5	2.4	2.5	2.5
	Piezoelectric Strain coefficients (pC/N)	$d_{14}$	42.8	45.8 #	47.7
Piezoelectric Stress coefficients (C/m <sup>2</sup> )	$e_{14}$	1.1	1.1	1.2	1.0
Coupling Factor (%)	$k_{14}$	32.8	–	36.3	–

\* The elastic compliance constants of BTO were calculated by the formula:  $s = c^{-1}$ ; #  $d_{14} = e_{14}/c_{44}^E$ .

In some studies, the piezoelectric coefficient was reported to be negative value for sillenite-type crystals [17]. The sign of  $d_{14}$  can be interpreted based on the crystal structure, where the M atom was coordinated by four oxygen atoms forming perfect tetrahedron, while the Bi atom with five neighbors of oxygen atoms forming an incomplete deformed  $\text{BiO}_5$  octahedron, with two additional electrostatically coordinated oxygen atoms on either side of the  $6s^2$  inert electron pair in  $\text{Bi}^{3+}$  [18,19], the polarity of the generated charges is controlled by the  $\text{MO}_4$  tetrahedron. In dextrorotatory  $\text{Bi}_{12}\text{MO}_{20}$ , the compressive stress applied along [111] direction deforms the tetrahedral O–M–O angles (no change in any M–O bond length), inducing a negative charge on the “M” side and a positive charge on the “O” side. So the directions of the positive piezoelectric effect correspond to the M→O directions in the  $\text{MO}_4$  tetrahedra, account for  $d_{14} > 0$ . If the  $\text{Bi}_{12}\text{MO}_{20}$  crystal is of opposite chirality, e.g., is laevorotatory, then  $d_{14} < 0$ , as shown in Figure 2 [1,2]. However, the magnitude of  $d_{14}$  is the same for dextrorotatory and laevorotatory crystals.

**Figure 2.** One unit cell of  $\text{Bi}_{12}\text{MO}_{20}$  showing the M–O tetrahedron and the polarization direction resulting from compression along [111]: (a) dextrorotatory; (b) laevorotatory [2] (Reprinted/Reproduced with permission from [2]. Copyright 1967 AIP Publishing LLC).



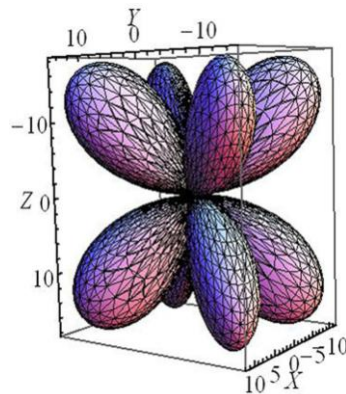
2.2. Orientation Dependence of Longitudinal Piezoelectric Coefficient

For cubic 23 symmetry, only face shear  $d_{14} = d_{25} = d_{36}$  exist. However, longitudinal coefficient  $d_{11} = d_{22} = d_{33}$  appears in the rotated coordinate. The orientation dependence of the longitudinal piezoelectric coefficient  $d_{33}^*$  was investigated. After a rotation of angle  $\alpha$  along the Z-axis then rotated  $\beta$  along the X-axis, piezoelectric coefficient  $d_{33}^*$  in the new coordinate can be determined according to the following equation:

$$d_{33}^* = 3d_{14} \sin\alpha \cos\alpha \sin^2\beta \cos\beta \tag{1}$$

Figure 3 shows the orientation dependence of longitudinal piezoelectric coefficient  $d_{33}^*$ , where the highest  $d_{33}^*$  was achieved for the ZX-cut (as shown in Figure 4a) rotated 45° around Z-axis (as shown in Figure 4b) then rotated 54° around X-axis (as shown in Figure 4c), refer to as ZXt/45°/54°-cut. Figure 4 illustrates the detailed rotational process of the ZXt/45°/54°-cut.

**Figure 3.** The orientation dependence of piezoelectric coefficient  $d_{33}^*$  for sillenite crystals.



The highest  $d_{33}^*$  direction was found along the [111] crystallographic direction, equivalent to  $\alpha = 45^\circ$  and  $\beta = 54^\circ$ , so [111] oriented longitudinal bars were prepared and the value of  $d_{33}^{[111]}$  was calculated using the following equations:

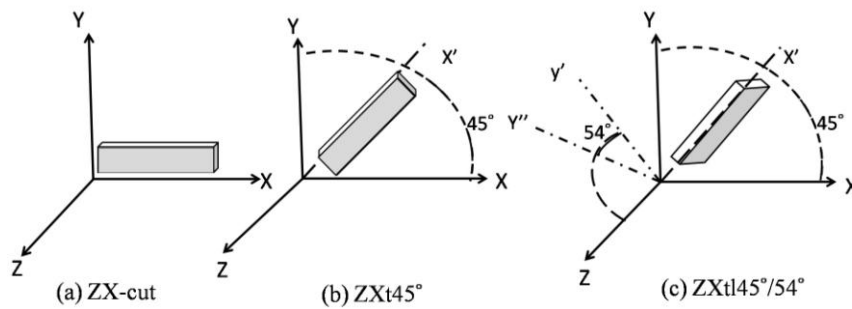
$$k_{33}^{[111]^2} = \frac{\pi f_r}{2 f_a} \cot\left(\frac{\pi f_r}{2 f_a}\right) \tag{2}$$

$$s_{33}^{E'} = \frac{1}{4\rho(l \cdot f_a)^2 (1 - k^2)} \tag{3}$$

$$d_{33}^{[111]} = k_{33}^{[111]} (s_{33}^{E'} \epsilon_{33})^{\frac{1}{2}} \tag{4}$$

$s_{33}^E$  is the short circuit elastic constant (measured in zero or constant field),  $s_{33}^{E'}$  is the short circuit elastic constant in the new coordinate system. The theoretical value of  $d_{33}^{[111]}$  was calculated based on Equation (1) and found to be 24.7 and 27.5 pC/N for BTO and BSO, respectively, in good agreement with the measured results of 25.5 and 28.1 pC/N based on the IEEE Standards [20].

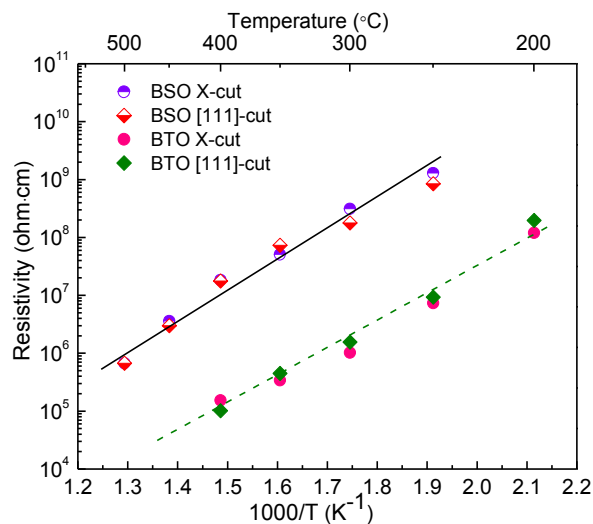
**Figure 4.** The coordinate rotation for ZXt45°/54°-crystal cut.



### 2.3. Temperature Dependence of the Electrical Resistivity

The electrical resistivity as a function of temperature for BTO and BSO crystals are plotted in Figure 5, exhibiting the expected Arrhenius behavior, where the activation energy  $E_a$  can be calculated from the slope of the lines, being on the order of 0.97 and 1.18 eV for BTO and BSO, respectively. There is no obvious difference observed for the electrical resistivities along X- and ZXt45°/54°-cut for both BTO and BSO crystals. The resistivity of BSO crystals was found to be two orders higher than that of BTO crystals, with the values being on the order of  $7 \times 10^5 \Omega \cdot \text{cm}$  at 500 °C.

**Figure 5.** Resistivity as a function of temperature for BTO and BSO crystals.



#### 2.4. Temperature Dependence of Dielectric and Piezoelectric Properties

Figure 6 shows the dielectric constant (relative dielectric permittivity) and dielectric loss (the insets in Figure 6) as a function of temperature (measured at 100 kHz) for BTO and BSO crystals. The dielectric constant of BTO along X- and [111]-direction was found to increase slightly from 47.6 to 48.8 with increasing temperature up to 350 °C, with the variation being less than 3%, as shown in Figure 6a. The dielectric loss of BTO was found to maintain low values, being <5% with temperature up to 250 °C, above which, the loss increased quickly to 30% at 350 °C, due to the increased ionic conduction. On the other hand, the dielectric constant of BSO (as show in Figure 6b) was found to be 48.2 and 48.7 along X- and [111]-direction at room temperature, slightly decreased in the low temperature range and then increased with increasing temperature, with overturn temperature being at 225 °C, the variation over temperature range of 20–500 °C is less than 1%, exhibiting very high thermal stability. Meanwhile, the dielectric loss of BSO was found to follow the same trend to that of BTO, with minimal variation in the range of 20–350 °C, then quickly increased to 20%–30% at the temperature of 500 °C.

**Figure 6.** Dielectric behaviors as a function of temperature for BTO and BSO crystals.

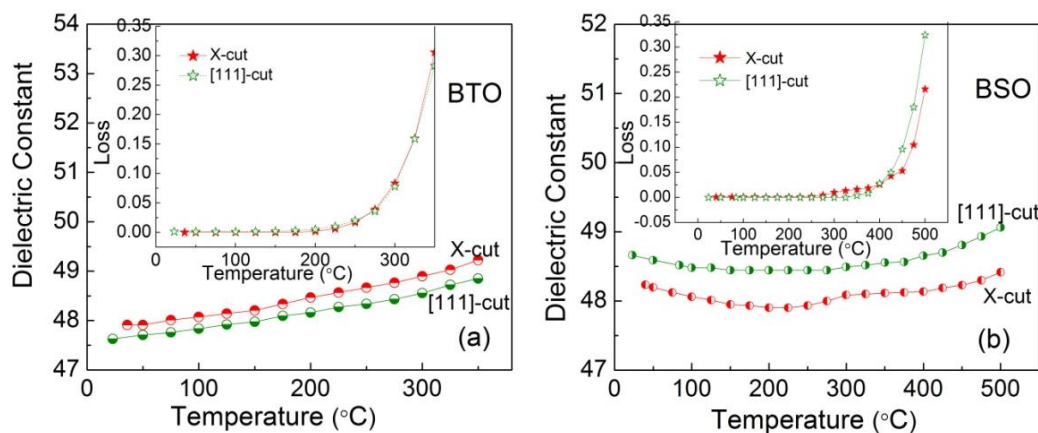


Figure 7 presents the temperature dependence of elastic compliance of BTO and BSO. From Figure 7a, elastic compliance constants  $s_{11}$ ,  $s_{12}$  and  $s_{33}^{[111]}$  of BTO were found to maintain the same values in the temperature range of 25–350 °C, while  $s_{44}$  was found to increase linearly from 40.3 to 44.1 pm<sup>2</sup>/N with increasing temperature, with the variation of <9%. As shown in Figure 7b, elastic constants  $s_{11}$  and  $s_{33}^{[111]}$  of BSO were found to increase slightly with increasing temperature, while  $s_{12}$  shows an opposite trend. In addition, elastic constants  $s_{44}$  was found to increase linearly from 40.4 to 45.1 pm<sup>2</sup>/N over 25–500 °C, with the variation being on the order of 12%.

Figure 8 exhibits the temperature characteristics of piezoelectric coefficients. As observed from Figure 8a, the piezoelectric coefficient  $d_{14}$  of BTO was found to increase from 42.8 to 44.1 pC/N with temperature increasing to 350 °C, with the variation of 3%, while  $d_{33}^{[111]}$  was found to maintain similar value. From Figure 8b, the piezoelectric coefficients  $d_{14}$  and  $d_{33}^{[111]}$  of BSO were found to decrease slightly as a function of temperature, with the overall variations of less than 6%. The above results demonstrate that both crystals exhibit high thermal stability of piezoelectric properties in the studied temperature ranges.

Figure 7. Elastic compliance as a function of temperature for BTO and BSO crystals.

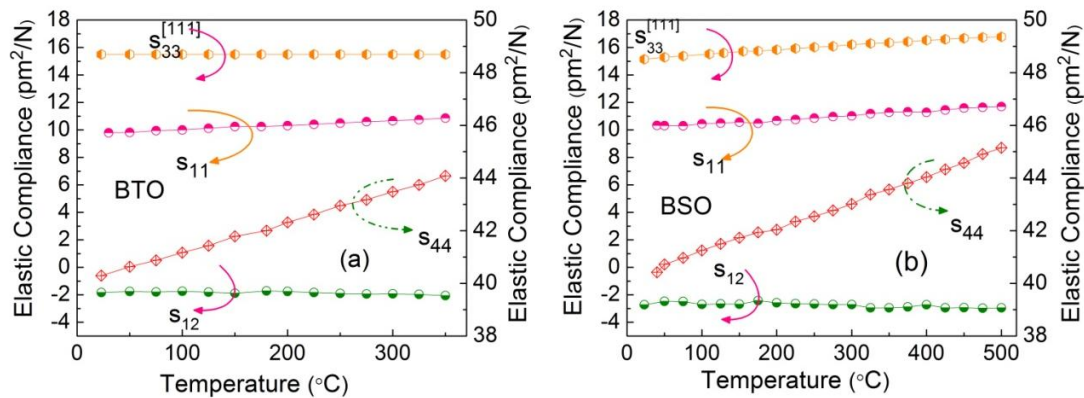
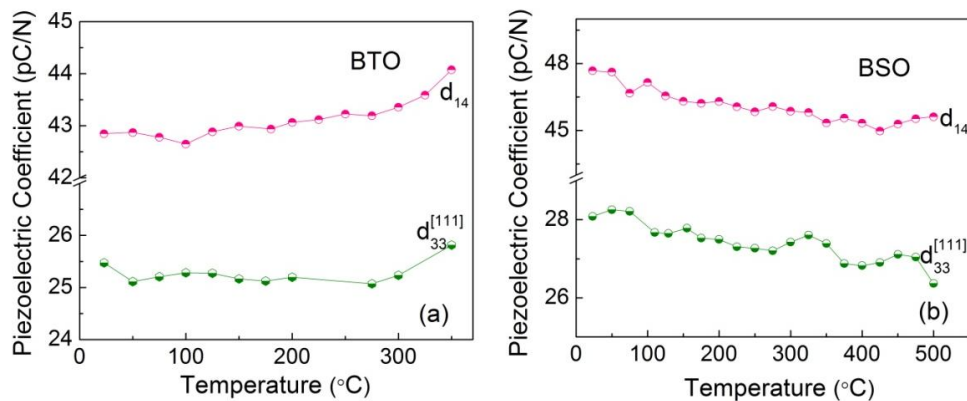
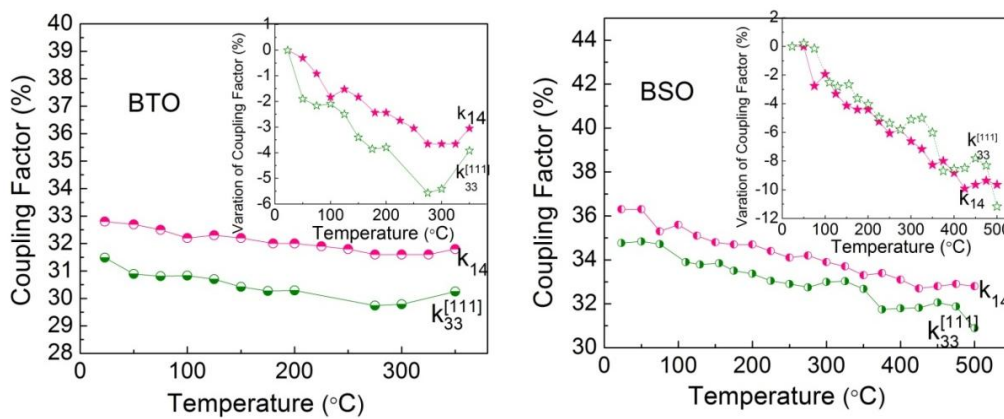


Figure 8. Piezoelectric coefficients as a function of temperature for BTO and BSO crystals.



The coupling factors as a function of temperature are given in Figure 9. From which, the coupling factor  $k_{14}$  and  $k_{33}^{[111]}$  are found to decrease slightly with increasing temperature, with the variations being less than 6% and 12% for BTO and BSO, respectively, as given in the small inset of Figure 9.

Figure 9. Coupling factor as a function of temperature for BTO and BSO crystals.



### 3. Experimental Section

Raw materials of Bi<sub>2</sub>O<sub>3</sub>, TiO<sub>2</sub>, SiO<sub>2</sub> and Nd<sub>2</sub>O<sub>3</sub> were used to grow Bi<sub>12</sub>TiO<sub>20</sub> and Nd<sub>0.06</sub>Bi<sub>11.94</sub>SiO<sub>20</sub> single crystals by the Czochralski technique. The crystals can be grown from congruent melt above

their melting points of 880–900 °C. It is important to point out that BTO is non-congruent melting, an excess of Bi<sub>2</sub>O<sub>3</sub> was added to the starting materials as self-solvent. The detailed crystal growth process was given in reference [16,21].

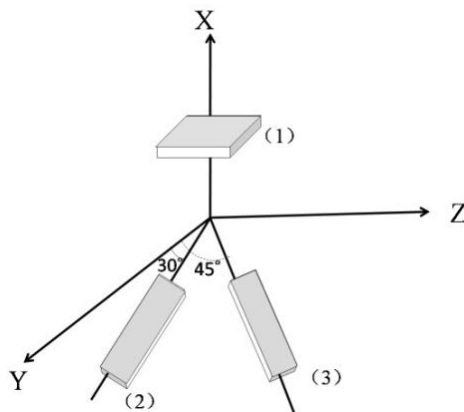
For sillenite-type crystals with cubic symmetry, there are 5 nonzero independent material constants, as shown in Equations (5)–(7). A schematic of the samples used for electrical measurements with different orientations is shown in Figure 10, the dimensions of the samples were 6 × 6 × 1.5 mm<sup>3</sup> for X-cut square plate and 12 × 4 × 1.5 mm<sup>3</sup> for long stripes, two to three samples were prepared for every crystal cuts. All the samples were vacuum sputtered with 200 nm platinum thin films on the large faces as electrodes. The resonance and anti-resonance frequencies were measured for determination of the material constants based on IEEE standards [20], using an Agilent HP 4194A impedance/gain-phase analyzer (Agilent Technology Inc., Santa Clara, CA, USA). The electrical resistivity was measured by two-probe method in the temperature range of 200 to 500 °C, using a source meter (Keithley 2410C, MetricTest, Hayward, CA, USA) with an applied voltage of ±50 V.

$$\epsilon = \begin{bmatrix} \epsilon_{11} & 0 & 0 \\ 0 & \epsilon_{11} & 0 \\ 0 & 0 & \epsilon_{11} \end{bmatrix} \tag{5}$$

$$d = \begin{bmatrix} 0 & 0 & 0 & d_{14} & 0 & 0 \\ 0 & 0 & 0 & 0 & d_{14} & 0 \\ 0 & 0 & 0 & 0 & 0 & d_{14} \end{bmatrix} \tag{6}$$

$$s = \begin{bmatrix} s_{11} & s_{12} & s_{12} & 0 & 0 & 0 \\ s_{12} & s_{11} & s_{12} & 0 & 0 & 0 \\ s_{12} & s_{12} & s_{11} & 0 & 0 & 0 \\ 0 & 0 & 0 & s_{44} & 0 & 0 \\ 0 & 0 & 0 & 0 & s_{44} & 0 \\ 0 & 0 & 0 & 0 & 0 & s_{44} \end{bmatrix} \tag{7}$$

**Figure 10.** Orientation of samples: (1) X-cut; (2) XYt30°; (3) XYt45°.



The capacitance  $C_p$  was measured on X-cut plate at 100 kHz frequency, the dielectric constant can be calculated using the following formula:

$$\epsilon_{11}^T / \epsilon_0 = \frac{C_p \cdot t}{A \cdot \epsilon_0} \tag{8}$$

$t$  is the thickness and  $A$  the area of the sample.

The length extension vibration can be excited in the long strips of  $XY\text{t}30^\circ$  and  $XY\text{t}45^\circ$  samples, to obtain  $s_{11}^E$ ,  $(2s_{12}^E + s_{44}^E)$  and  $d_{14}$  by the following equations:

$$s_{22}^{E'} = \frac{1}{4\rho(l \cdot f_r)^2} \quad (9)$$

$$s_{22}^{E'} = s_{11}^E(\sin^4\theta + \cos^4\theta) + (2s_{12}^E + s_{44}^E)\sin^2\theta\cos^2\theta \quad (10)$$

$$\frac{k_{12}'^2}{k_{12}'^2 - 1} = \frac{\pi f_a}{2 f_r} \cot\left(\frac{\pi}{2} \times \frac{f_a}{f_r}\right) \quad (11)$$

$$d_{12}' = k_{12}'(s_{22}^{E'}\varepsilon_{11}^T)^{\frac{1}{2}} \quad (12)$$

$$d_{14} = d_{12}'/(\sin\theta \cos\theta) \quad (13)$$

$$k_{14} = d_{14}' / (s_{44}^E\varepsilon_{11}^T)^{\frac{1}{2}} \quad (14)$$

$f_r$  is the resonance frequency,  $l$  the length of sample,  $\rho$  the density: being 9.1 and 9.2 g/cm<sup>3</sup> for BTO and BSO, respectively.

$s_{44}^E$  can be determined by measuring the resonance frequency of  $X$ -cut square plate [22,23]:

$$s_{44}^E = \frac{F^2}{4\rho(l \cdot f_r)^2} \quad (15)$$

$$F = \frac{2k_0\alpha}{\pi} \quad (16)$$

Here  $F$  is a correction constant,  $k_0$  is a root of the equation:  $\tan k_0 + k_0 = 0$ , with the first root equals to 2.0288 and  $\alpha = 1 - 0.05015 \times [(s_{22}^E + s_{33}^E)/2s_{44}^E]^{\frac{1}{2}}$ .

After obtaining the elastic constant  $s_{44}^E$ , the value of  $s_{12}^E$  can be calculated from  $(2s_{12}^E + s_{44}^E)$  according to Equation (10), finally, the  $k_{14}$  can be calculated by Equation of (14).

On the other hand, the  $d_{14}$  and  $k_{14}$  can be directly determined by measuring the face shear square plate [22–25]:

$$k_{14}^2 = \frac{1}{1 + rp\chi} \quad (17)$$

$$p = \frac{4\alpha^2}{(k_0^2 + 2)} [1 - 0.0691 \times (\frac{s_{22}^E + s_{33}^E}{2s_{44}^E})] \quad (18)$$

$$\frac{1}{r} = \frac{f_a^2 - f_r^2}{f_r^2} \quad (19)$$

$$d_{14} = k_{14} (s_{44}^E\varepsilon_{11}^T)^{\frac{1}{2}} \quad (20)$$

$\chi \approx 1$  for face shear mode,  $p$  is a correction constant,  $f_a$  the anti-resonance frequency.

#### 4. Conclusions

The full matrix of electro-elastic constants of BTO and BSO crystals were determined, with  $d_{14}$  and  $k_{14}$  of 40–48 pC/N and 31%–36%, respectively, based on which, the highest double rotated  $d_{33}^*$  was achieved in [111] crystallographic direction, being on the order of 25~28 pC/N. The electrical

resistivity of BSO was found to be on the order of  $7 \times 10^5 \Omega \cdot \text{cm}$  at 500 °C, two orders higher than that of BTO. Of particular importance is that both BTO and BSO crystals shown high thermal stability of piezoelectric properties over the temperature range of 25–350 and 25–500 °C, respectively, with the variations of <6%, demonstrating that the sillenite-type crystals are potential piezoelectric materials for electromechanical applications in a medium temperature range.

### Acknowledgments

The authors would like to thank Thomas R. Shrout for the helpful discussion. The author Chuanying Shen acknowledged the financial support from the China Scholarship Council.

### Author Contributions

The experiments were designed by Chuanying Shen, Huaijin Zhang and Shujun Zhang; Chuanying Shen performed the experiments; Chuanying Shen, Huaijin Zhang and Shujun Zhang prepared the manuscript. All authors discussed the results and contributed to the refinement of the paper.

### Conflicts of Interest

The authors declare no conflict of interest.

### References

1. Abrahams, S.C.; Jamieson, P.B.; Bernstein, J.L. Crystal Structure of Piezoelectric Bismuth Germanium Oxide  $\text{Bi}_{12}\text{GeO}_{20}$ . *J. Chem. Phys.* **1967**, *47*, 4034–4041.
2. Abrahams, S.C.; Bernstein, J.L.; Svensson, C. Crystal structure and absolute piezoelectric  $d_{14}$  coefficient in laevorotatory  $\text{Bi}_{12}\text{SiO}_{20}$ . *J. Chem. Phys.* **1979**, *71*, 788–792.
3. Sillén, L.G. X-ray Studies on Oxides and Oxyhalides of Trivalent Bismuth. Inaugural Dissertation, Degree-Granting University, Stockholm, Sweden, 1940.
4. Efendiev, S.M.; Kulieva, T.Z.; Lomonov, V.A.; Chiragov, M.I.; Grandolfo, M.; Vecchia, P. Crystal Structure of Bismuth Titanium Oxide  $\text{Bi}_{12}\text{TiO}_{20}$ . *Phys. Status Solidi A* **1981**, *74*, K17–K21.
5. Wiehl, L.; Friedrich, A.; Haussühl, E.; Morgenroth, W.; Grzechnik, A.; Friese, K.; Winkler, B.; Refson, K.; Milman, V. Structural compression and vibrational properties of  $\text{Bi}_{12}\text{SiO}_{20}$  sillenite from experiment and theory. *J. Phys. Condens. Matter* **2010**, *22*, 505401:1–505401:50.
6. Aldrich, R.E.; Hou, S.L.; Harvill, M.L. Electrical and Optical Properties of  $\text{Bi}_{12}\text{SiO}_{20}$ . *J. Appl. Phys.* **1971**, *42*, 493–494.
7. Peltier, M.; Micheron, F. Volume hologram recording and charge transfer process in  $\text{Bi}_{12}\text{SiO}_{20}$  and  $\text{Bi}_{12}\text{GeO}_{20}$ . *J. Appl. Phys.* **1977**, *48*, 3683–3690.
8. Burimov, N.; Mandel, A.; Reshet'ko, A.; Shandarov, S.; Volkov, V.; Kargin, Yu. Elastic and piezoelectric constants of  $\text{Bi}_{12}\text{TiO}_{20}$  crystals. *Opt. Mater.* **1995**, *4*, 179–181.
9. Vasconcelos, I.F.; Pimenta, M.A.; Sombra, A.S.B. Optical properties of  $\text{Bi}_{12}\text{SiO}_{20}$  (BSO) and  $\text{Bi}_{12}\text{TiO}_{20}$  (BTO) obtained by mechanical alloying. *J. Mater. Sci.* **2001**, *36*, 587–592.
10. Günter, P.; Huignard, J.P. *Photo-refractive Materials and their Applications*; Springer Verlag: Berlin, Germany, 1988; Volume I.

11. Coxa, C.; Zaldo, C.; Volkov, V.V.; Egorysheva, A.V.; Polgár, K.; Péter, A. Gallium-induced inhibition of the photorefractive properties of sillenite crystals. *J. Opt. Soc. Am. B* **1996**, *13*, 908–991.
12. Buse, K. Light-induced charge transport processes in photorefractive crystals I: Models and experimental methods. *Appl. Phys. B* **1997**, *64*, 273–291.
13. Schweppe, H.; Quadflieg, P. Electromechanical Properties of Bismuth Silicon Oxide ( $\text{Bi}_{12}\text{SiO}_{20}$ ). *IEEE Trans. Sonics Ultrason.* **1974**, *21*, 56–57.
14. Papazoglou, D.G.; Apostolidis, A.G.; Vanidhis, E.D. Measurement of the electro-optic coefficient of  $\text{Bi}_{12}\text{GeO}_{20}$  (BGO),  $\text{Bi}_{12}\text{TiO}_{20}$  (BTO) crystals. *Synth. Met.* **1996**, *83*, 281–285.
15. Kamenov, V.P.; Shamonina, E.; Ringhofer, K.H.; Nippolainen, E.; Prokofiev, V.V.; Kamshilin, A.A. Photorefractive light scattering families in 111-cut  $\text{Bi}_{12}\text{TiO}_{20}$  crystals with an external electric AC field. *Phys. Rev. E* **2000**, *63*, 016607:1–016607:6.
16. Xu, H.H.; Zhang, Y.Y.; Zhang, H.J.; Yu, H.H.; Pan, Z.B.; Wang, Y.C.; Sun, S.Q.; Wang, J.Y.; Boughton, R.I. Growth and characterization of  $\text{Nd}:\text{Bi}_{12}\text{SiO}_{20}$  single crystal. *Opt. Commun.* **2012**, *285*, 3961–3966.
17. Gorfman, S.; Hüsecken, A.; Burianek, M.; Mühlberg, M.; Pietsch, U. Investigation of microscopic origin of piezoelectric effect in  $\text{Bi}_{12}\text{SiO}_{20}$ . Available Online: [http://photon-science.desy.de/annual\\_report/files/2012/20122312.pdf](http://photon-science.desy.de/annual_report/files/2012/20122312.pdf) (accessed on 23 December 2012).
18. Wojdowski, W. Vibrational Modes in  $\text{Bi}_{12}\text{GeO}_{20}$  and  $\text{Bi}_{12}\text{SiO}_{20}$  Crystals. *Phys. Status Solidi B* **1985**, *130*, 121–130.
19. Neov, S.; Marinova, V.; Reehuis, M.; Sonntag, R. Neutron-diffraction study of  $\text{Bi}_{12}\text{MO}_{20}$  single crystals with sillenite structure ( $\text{M} = \text{Si}, \text{Si}_{0.995}\text{Mn}_{0.005}, \text{Bi}_{0.53}\text{Mn}_{0.47}$ ). *Appl. Phys. A* **2002**, *74*, S1016–S1018.
20. *IEEE Standard on Piezoelectricity*, ANSI/IEEE Std 176–1987; American Standards National Institute: New York, NY, USA, 1987.
21. Liao, H.B.; Xu, L.Y.; Liu, J.C. The crystal growth of  $\text{Bi}_{12}\text{TiO}_{20}$ . *J. Inorg. Mater.* **1994**, *3*, 257–267. (In Chinese)
22. Bechmann, R.; Fair, I.E. IRE standards on piezoelectric crystals: Determination of the elastic, piezoelectric, and dielectric constants- the electromechanical coupling factor. In Proceedings of the IRE, New York, NY, USA, 6–8 May 1958; Volume 46, pp. 764–778.
23. Bechmann, R. Contour modes of square plates excited piezoelectrically and Determination of elastic and piezoelectric coefficients. *Proc. Phys. Soc. B* **1951**, *64*, 323–337.
24. Zhang, S.J.; Jiang, W.H.; Meyer, R.J., Jr.; Li, F.; Luo, J.; Cao, W.W. Measurements of face shear properties in relaxor- $\text{PbTiO}_3$  single crystals. *J. Appl. Phys.* **2011**, *110*, 064106:1–064106:6.
25. Mason, W.P. Elastic, piezoelectric and dielectric properties of sodium, chlorate and sodium bromated. *Phys. Rev.* **1946**, *70*, 529–537.